GEOPHYSICAL RESEARCH LETTERS, VOL. 17, NO. 7, PAGES 997-1000, JUNE 1990

FAULT PARAMETERS AND TSUNAMI EXCITATION OF THE MAY 23, 1989, MACQUARIE RIDGE EARTHQUAKE

Kenji Satake and Hiroo Kanamori

Seismological Laboratory, California Institute of Technology

Abstract. The Macquarie Ridge earthquake of May 23, 1989, is one of the largest events in the last decade. Furthermore, it is the largest strike-slip earthquake ever recorded instrumentally. We analyzed long-period surface waves and body waves recorded at global networks (GDSN, IRIS, GEOSCOPE, and IDA) to estimate the fault parameters and computed tsunamis from the estimated parameters. The Centroid Moment Tensor (CMT) solution from surface waves shows that the mechanism is almost pure strike-slip with one of the nodal planes parallel to the strike of the Macquarie Ridge. The seismic moment is 1.6×10^{21} Nm ($\times 10^{28}$ dyn·cm) and the corresponding moment magnitude is M_w=8.1. Teleseismic P and S waves from 10 stations with good azimuthal coverage are used to model the temporal and spatial distribution of the subevents. Four subevents are located sequentially from south to north along the ridge system in about 30 sec. All of them have a mechanism similar to the CMT solution. The fault length is estimated to be about 120 km from the subevent and the aftershock distributions. The rupture propagates from south to north at a relatively high speed. The average slip on the fault depends on the estimate of the fault width, but is probably larger than 9 m. A large strike-slip earthquake like this event produces significant vertical displacements on the ocean bottom and excites tsunamis. Computation of tsunamis using the estimated fault parameters predicts that small tsunamis are expected at Australia and New Zealand. In fact, small tsunamis were observed on the southern coast of Australia.

Introduction

A great earthquake occurred on the Macquarie Ridge, south of New Zealand on May 23, 1989. The epicentral parameters given by NEIS are the following: the origin time, 10:54:46.3 GMT; location, 52.341 °S, 160.568 °E; depth, 10 km; and M_S, 8.2. This earthquake is probably the largest event since the 1977 Indonesian (Sumba) earthquake (M_S 7.9, M_w 8.3) or the 1979 Colombia earthquake (M_S 7.7, M_w 8.2). As we will show in this paper, this event has a strike-slip mechanism. No strike-slip event of this size has been ever recorded instrumentally before. Another interesting feature of this event is that small tsunamis were observed on the southern coast of Australia despite the strike-slip mechanism of the earthquake.

The Macquarie Ridge extends south of New Zealand and forms a plate boundary between the Pacific and Australia plates. Large earthquakes which have occurred there in the past were extensively studied by Ruff et al. [1989]. They found that the mechanism of large events had bimodal distribution; either strike-slip along the ridge axis or dip-slip with the Australia plate subducting beneath the Pacific plate. Ruff et al.[1989] interpreted this complexity as an initiation of the subduction process in this region.

In this paper, we determine the fault parameters of the 1989 Macquarie Ridge earthquake, using seismic surface waves and body waves and compute tsunamis using fault models derived from the seismic data.

Paper number 90GL00714;
0094-8276/90/90GL-00714$03.00

Surface Wave Analysis

We made a Centroid Moment Tensor (CMT) inversion [Dziewonski et al., 1981; Kawakatsu, 1989] using long-period surface waveforms recorded at 11 stations of the GDSN and the IRIS network. We used R1, R2 and G1, G2 at AFI, ANTO, BCAO, BJI, CMB, CTAO, KEV, MDJ, WMQ (GDSN), PAS, and HRV (IRIS). At five stations (AFI, BJI, KEV, MDJ, and WMQ), R1 and G1 are off-scale and could not be used. The azimuthal coverage of the stations is fairly good if we consider the symmetrical nature of surface wave radiation pattern. We fixed the depth at 10 km in the earth model 1066A.

The result of CMT inversion is summarized in Table 1. The T-axis is 1.8×10^{21} Nm (pl. 27 °, az. 350 °), the P-axis is 1.4×10^{21} Nm (pl. 9 °, az. 85 °), and the N-axis is 0.4×10^{21} Nm (pl. 62 °, az. 192 °). If we decompose this moment tensor into a best double couple and a CLVD, the best double couple has a scalar seismic moment of 1.6×10^{21} Nm. The deviation from double couple which is expressed by ϵ, the ratio of the minimum (absolute sense) to the maximum eigenvalue, is 0.23. The moment magnitude M_w is computed as 8.1 from the scalar moment. The mechanism of the best double couple is almost pure strike-slip as shown in Figure 1. The nodal plane that is parallel to the Macquarie ridge axis is likely to be the fault plane.

Table 1. Centroid moment tensor solution

Moment tensor elements (10^{19}Nm)			
M_{rr}	0.8	±	1.7
$M_{\theta\theta}$	130.3	±	2.3
$M_{\phi\phi}$	-131.0	±	2.2
$M_{r\theta}$	86.8	±	12.7
$M_{r\phi}$	29.7	±	14.4
$M_{\theta\phi}$	37.2	±	1.7
best double couple			
M_0	(10^{19}Nm)		160
ϵ			0.23
ϕ	(strike)	131	35
δ	(dip)	65	78
λ	(slip)	13	154

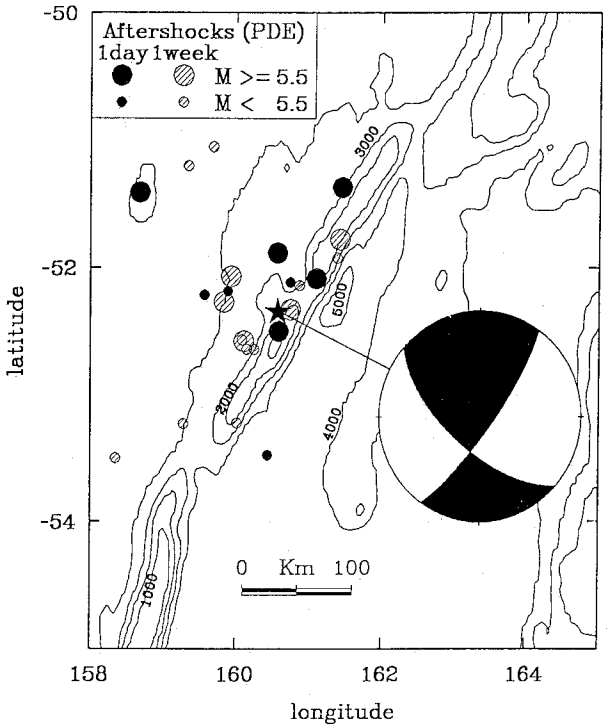

Fig. 1. Map of the source region and the aftershocks. The mechanism obtained from surface waves is shown. Contour interval for the ocean depth is 1000 m.

The motion on this plane is right-lateral. The centroid time is 30 sec, very small for an earthquake of this size. This solution is similar to that obtained by Dziewonski et al. [1990].

Body Wave Analysis

The GDSN stations usable for body wave analysis (i.e., distance range of 30° and 100°) are very few, especially in some azimuths. We used the records from the GEOSCOPE [Romanowicz et al., 1984] and IDA [Agnew et al., 1986] networks in conjunction with the GDSN records. By combining the above three network stations, the station coverage becomes very good. We use P and S waves recorded on a broadband channel (one of BRB, VBB, BB, or MH). All the records are first deconvolved with their individual response, convolved with the WWSSN (LP) response, and decimated at 1 sec intervals. Thus the waveforms from different networks can be directly compared to each other. Figure 2 shows the P and SH waveforms with station locations plotted on a focal sphere.

We applied a multiple deconvolution method of P and SH waves [Kikuchi and Kanamori, 1989]. In this method, the observed seismograms are matched by synthetic seismograms computed for a sequence of subevents distributed on the fault plane. We compute Green's functions for five independent moment tensor elements, and represent the waveform by a linear combination of the Green's functions from subevents. By minimizing the difference between the observed and synthetic seismograms, we determine the moment tensor or mechanism of each subevent as well as their spatial and temporal location.

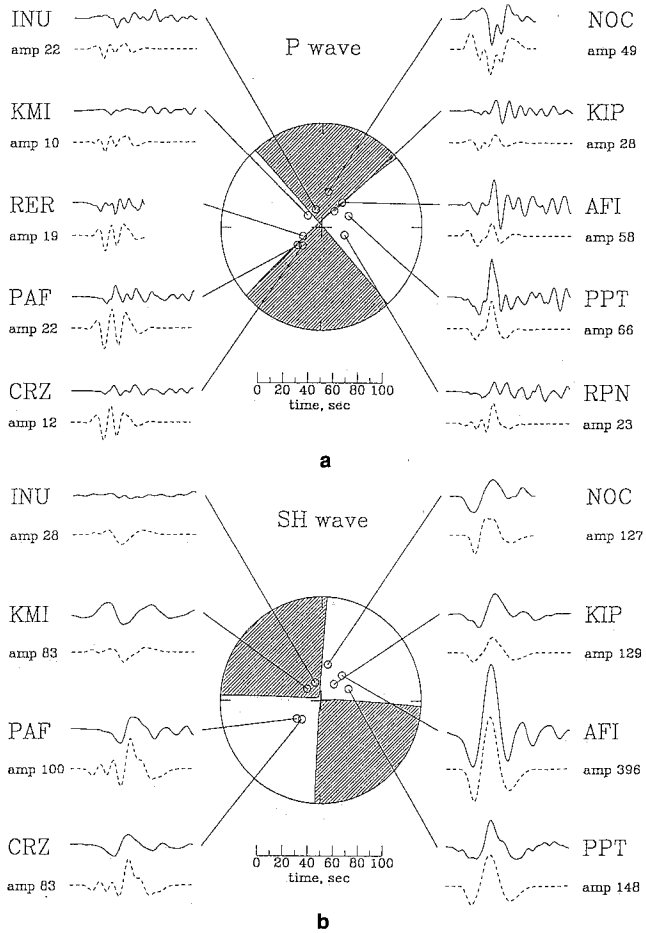

Fig. 2. Observed (solid lines) and synthetic (dashed lines) body waveforms for P wave (a) and SH wave(b). Mechanism solution of the largest subevent is shown in the focal sphere. Peak-to-peak amplitude in cm for WWSSN response with gain 1500 are shown.

The point sources are distributed in the strike direction (35°) determined from the CMT solution with an interval of 20 km. The Green's functions are computed from each point source for a simple earth model consisting of a water layer (2 km thick), crust, and mantle. We fix the depth at 10 km since the depth resolution of body wave is generally poor and there is a trade-off between depth and moment estimates. The source time function for each subevent is assumed to be a triangle with rise and fall times of 5 sec respectively.

The result of the deconvolution is summarized in Figure 3 and Table 2. Only four major subevents are shown. All the subevents show a strike-slip mechanism similar to that obtained from surface waves. The four subevents are located successively from south to north at 40 km interval and the total extent is about 120 km. Deviation from a double couple is fairly small for all subevents except No. 2. The total time duration for the four subevents is about 30 sec. Apparently the rupture propagated towards the north with a rupture velocity of about 4 km/s. The sum of the seismic moments of the four subevents is 1.1×10^{21} Nm, which is slightly smaller than that from surface waves. The difference is probably due to the difference in period between surface and body waves.

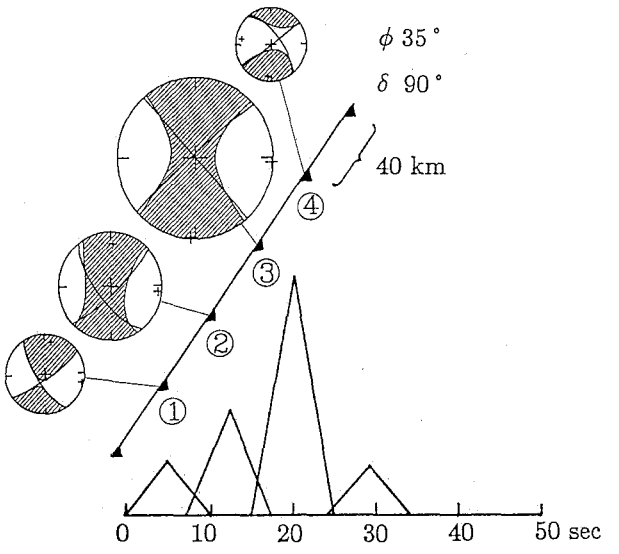

Fig. 3. The mechanisms, time functions, and distribution of subevents.

Table 2. Parameters of subevents

No.	1	2	3	4
time (s)	0	7	15	24
$M_0(10^{19}\mathrm{Nm})$	13	25	58	12
ϵ	-0.01	0.36	0.18	-0.22
ϕ_1	57	48	228	54
δ_1	80	80	87	89
λ_1	162	157	180	-157
ϕ_2	150	142	318	324
δ_2	73	68	90	67
λ_2	11	11	3	-1

Fault Parameters

To estimate the fault parameters such as length L, width W, the average slip D, and static stress drop $\Delta\sigma$, we need seismic or geological information other than the seismic moment, because seismic moment merely gives a product of L, W, D, and the rigidity μ. The fault length can be estimated to be about 120 km from the subevent distribution obtained in the last section. The aftershock distribution seems to support this estimate too. The aftershocks located by PDE are shown in Figure 1. The epicenters are very scattered off the ridge axis, partly because of the poorly determined location for this remote earthquake. Four larger events are located right on the ridge over a distance of about 100 km. Two events just off the ridge are at the northern and southern extension. If we include them, the aftershock zone may be near 200 km long. In any case, the aftershock zone is abnormally short for the earthquake size.

The fault width is difficult to estimate particularly for a remote earthquake such as this event. Empirical relationships from many large earthquakes show that the aspect ratio (L/W) is roughly constant and approximately 2. If we apply this to the present case, the width is estimated to be 60 km. Since the dip angle is almost 90°, this requires that the fault extends as far deep as 60 km. It is very unlikely that this event cuts the upper mantle at such a depth. The depths of all the aftershocks shown in Figure 1 are constrained at 10 km but they are probably shallow. For large strike-slip earthquakes, such as the 1906 San Francisco earthquake and the 1976 Guatemala earthquake, the aspect ratio is much larger, about 20. Here we assume W=10 to 30 km. This depth range appears more reasonable for the depth extent of faulting.

If the fault area is 120 × 10 to 120 × 30 km^2, the average slip, computed from the seismic moment assuming a rigidity of 5×10^{11} dyne/cm^2 ($\times10^{10}$ Pa), is 27 to 9 m. The static stress drop for a strike-slip fault can be computed as $\Delta\sigma = (2/\pi)\mu(D/W) = (2/\pi)(M_0/LW^2)$. This gives an estimate of 850 to 90 bars (8.5 to 0.9 $\times10^7$ Pa), significantly higher than the average for inter-plate earthquakes. A strike-slip fault produces vertical uplift and subsidence near the end of the fault. The maximum uplift and subsidence for a fault with D=9 m and W= 30 km are about 50 cm.

Tsunami Generation

There seems to be a common misconception that tsunamis are not generated by a strike-slip earthquake. Both observation and theory showed that this is not the case. The North Atlantic earthquake of 1975, a strike-slip event, generated observable tsunamis [Lynnes and Ruff, 1985]. Tsunamis were also recorded from the 1906 San Francisco earthquake. The tide gauge record at Fort Point (San Francisco) shows a very distinct arrival of tsunami with an amplitude of 10 cm. Ward [1982] and Okal [1988] computed excitation of tsunamis theoretically for several types of mechanisms, using normal mode theory and assuming that the ocean depth is uniform. They showed that the tsunami amplitude for a strike-slip source is about a factor of 3 to 4 smaller than that for a dip-slip source.

We modeled and computed the generation and propagation of tsunamis from this earthquake. Using the vertical crustal displacement field computed from the fault parameters as the initial condition, tsunamis are computed by a finite-difference method for the actual bathymetry. The grid size of the bathymetric data is 5 min. Tsunami waveforms are computed at several points. Figure 4 shows the computed tsunami waveforms at Sydney, Australia and Wellington, New Zealand. Computed tsunamis arrive at these stations

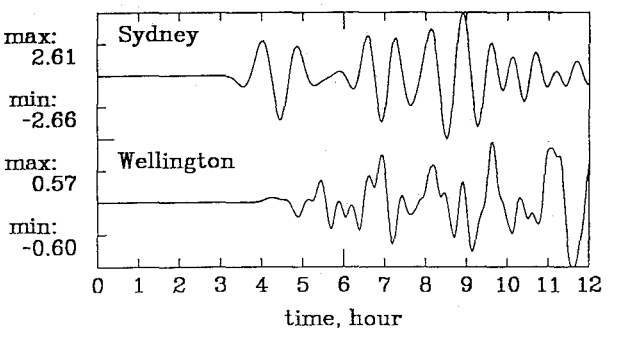

Fig. 4. Tsunami waveforms computed for the fault model with W=30 km. The maximum and minimum amplitudes are shown in cm.

about 3 to 4 hours after the origin time. The amplitudes are very small; 2 to 5 cm at Australian stations and less than 1 cm at New Zealand stations.

Tsunamis from this event were recorded at least at four tide gauge stations in southeastern Australia, southeast Tasmania and southeastern New South Wales [McCue, 1990]. The maximum peak-to-trough amplitude is reported to be 30 cm. We examined 12 tide gauge records from New Zealand but could not identify any tsunamis more than a few cm in amplitude. These observations suggest strong directivity for tsunami excitation; relatively large tsunamis at Australia compared to New Zealand. This tendency can be seen in the above computation. However, the amplitude of 30 cm on the Australian coast seems much larger than expected from our source model with W=30 km, even if we take into account local resonance at the harbor or bay. If we use W=10 km, the estimated tsunami height would be approximately three times larger, and is comparable to that reported in Australia. We need to further examine tide gauge records from these stations before we constrain the fault model from tsunami data.

Conclusion

Seismological observation of the Macquarie Ridge earthquake shows that the duration and fault size are very small for an event with M_W=8.1. A large slip (more than 9 m) on the fault plane is required to explain the seismic moment. This large slip produces a large amount of uplift and subsidence at the edge of the fault which excites tsunamis. More data, particularly tsunami records from Australia, will help to better constrain the fault model and clarify the source process of this unusual earthquake.

Acknowledgements. We thank Barbara Romanowicz and Göran Ekström for providing us with GEOSCOPE data, Helen Anderson and Terry Webb for providing us with tide gauge data from New Zealand and related information, and Heidi Houston for reviewing the manuscript. This work was supported by USGS grant No 14-08-001-G1356 and NSF grant EAR-89-15987. KS is supported by Fellowship for Research Abroad from Japan Society for the Promotion of Science. Contribution No. 4833, Division of Geological and Planetary Sciences, California Institute of Technology.

References

Agnew, D.C., J. Berger, W.F. Farrell, J.F. Gilbert, G. Masters and D. Miller, Project IDA: A decade in review, *EOS, 67*, 203-212, 1986.

Dziewonski, A.M., T.-A. Chou and J.H. Woodhouse, Determination of earthquake source parameters from waveform data for studies of global and regional seismicity, *J. Geophys. Res., 86*, 2825-2852, 1981.

Dziewonski, A.M., G. Ekström, J. H. Woodhouse and G. Zwart, Centroid-moment tensor solutions for April - June, 1989, *Phys. Earth Planet. Inter., (in press)*, 1990.

Kawakatsu, H., Centroid single force inversion of seismic waves generated by landslides, *J. Geophys. Res., 94*, 12363-12374, 1989.

Kikuchi, M. and H. Kanamori, Analysis of multiple events with mechanism changes, *Progr. Abst. Seism. Soc. Japan, 1*, 3, 1989.

Lynnes, C.S. and L.J. Ruff, Source process and tectonic implications of the great 1975 North Atlantic earthquake, *Geophys. J. R. astr. Soc., 82*, 497-510, 1985.

McCue, K., Earthquake update, *EOS, 71*, 2, 1990.

Okal, E., Seismic parameters controlling far-field tsunami amplitudes: A review, *Natural Hazards, 1*, 67-96, 1988.

Romanowicz, B., M. Cara, J.F. Fels and D. Rouland, GEOSCOPE: A French initiative in long-period three-component global seismic networks, *EOS, 65*, 753-754, 1984.

Ruff, L.J., J.W. Given, C.O. Sanders and C.M. Sperber, Large earthquakes in the Macquarie Ridge Complex: Transitional tectonics and subduction initiation, *PAGEOPH, 129*, 71-129, 1989.

Ward, S., On tsunami nucleation. II. An instantaneous modulated line source, *Phys. Planet. Earth Inter., 27*, 273-285, 1982.

K. Satake and H. Kanamori, Seismological Laboratory, California Institute of Technology, Pasadena, CA 91125.

(Received January 31, 1990;
accepted March 15, 1990)